

## THE PERFORMANCE OF DISCRETE MODELS OF LOW REYNOLDS NUMBER SWIMMERS

QIXUAN WANG<sup>†</sup>

Department of Mathematics  
University of California Irvine  
Irvine, CA

HANS G. OTHMER<sup>‡</sup>

School of Mathematics  
University of Minnesota  
Minneapolis, MN 55445, USA

(Communicated by ???)

**ABSTRACT.** Swimming by shape changes at low Reynolds number is widely used in biology and understanding how the efficiency of movement depends on the geometric pattern of shape changes is important to understand swimming of microorganisms and in designing low Reynolds number swimming models. The simplest models of shape changes are those that comprise a series of linked spheres that can change their separation and/or their size. Herein we compare the efficiency of three models in which these modes are used in different ways.

**1. Introduction.** Single-cell organisms use a variety of strategies for translocation, including crawling, swimming, drifting with the surrounding flow, and others. Some, such as bacteria, use flagella, and others, such as paramecia, use cilia to swim, and both types use only one mode. However other cells can be more flexible in that they either crawl by transient attachments to their surroundings – often called the mesenchymal mode, or by shape changes – called the amoeboid mode [13]. The former may involve strong adhesion to the substrate or the extracellular matrix (ECM) via integrin-mediated adhesion complexes, while the latter depends less on force transmission to the ECM or to the surrounding fluid, and instead involves shape changes to exploit spaces in the ECM to move through it (*cf.* Fig. 1). The latter mode can be far more effective and can lead to speeds up to forty times faster than those resulting from mesenchymal motion [37]. Cells such as leukocytes, which normally use the mesenchymal mode in the ECM, can migrate *in vivo* in the absence of integrins, using a 'flowing and squeezing' mechanism [25]. While crawling and swimming are mechanistically distinct strategies, cells can sense their environment and use the most efficient strategy in a given context.

The spatio-temporal scale of motion of small organisms in viscous fluids frequently leads to low Reynolds number (LRN) flows. Swimmers that use a single long, thin flagellum led to the development and application of slender-body theory

---

2010 *Mathematics Subject Classification.* Primary: 92C45, 92C50; Secondary: 92B05.

*Key words and phrases.* Cell motility, swimming, Low Reynolds number flows.

<sup>†</sup> <sup>‡</sup>H. G. Othmer is supported in part by NIH Grant # GM29123-36 and NSF Grant # 1311974

"Any opinions, findings, and conclusions or recommendations expressed in this material are those of the author(s) and do not necessarily reflect the views of the National Science Foundation." .

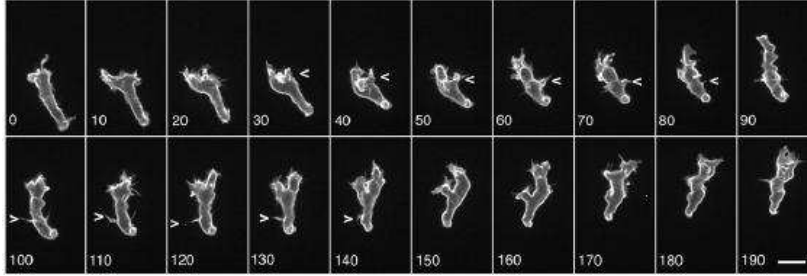


Figure 1: A sequence of shape changes observed in a *Dictyostelium discoideum* cell swimming in a fluid [9].

[27, 20, 22, 16, 11, 23, 21], while microorganisms that swim using a thin layer of cilia were first studied by Lighthill for squirming motion of nearly spherical deformable bodies [28]. A general review of previous work on swimming appears in [26], and here we only analyze models that comprise a number of linked subunits and have only a finite number of degrees of freedom. We call these discrete models of swimmers.

Much of the current interest in locomotion at LRN was stimulated by Purcell's description of life at low Reynolds number [35]. In particular, the observation that certain classes of shape changes produce no net motion in a viscous fluid led to studies on various types of discrete models of swimmers, with the goals of understanding how microorganisms swim and facilitating the design of mini-robots that swim at LRN. The first discrete LRN model is *Purcell's two-hinge swimmer*, also referred to as *Purcell's three-link swimmer* [36] (Fig. 2 (a)). Purcell's model swimmer comprises three connected, rigid segments that are constrained to move in a plane and can execute restricted rotations around joints linking the segments. The shape is specified by two parameters, the angles between adjacent segments, and Purcell showed that one can impose sequences of changes in the angles that produce net translation of the swimmer. Despite its geometric simplicity, the relationships between geometric parameters, speed and efficiency of swimming are not simple [12, 6], but approximations of optimal strokes are known [39]. Various simpler linked-sphere models for which both analytical and computational results can be obtained have appeared since. The first of these is the Najafi-Golestanian three-sphere *accordion* model (NG) [30, 18, 1] (Fig. 2 (b)), which comprises three rigid spheres connected by two slender connecting arms aligned along the  $x$ -direction that can stretch and contract in a prescribed form to produce motion. Since the forces that expand or contract the arms are directed along them it can only result in translation – it never rotates. Another linked-sphere model is the *pushmepullyou* swimmer (PMPY) [7] (Fig. 2 (c)), in which two spheres that can expand or contract radially are connected by an extensible arm. Analytical and numerical studies of the NG and PMPY models have been done heretofore, and their efficiency and the optimality of various strokes have been investigated [2, 3, 4]. Recently we have analyzed a three-sphere volume-exchange or *breather* model (VE) in which the spheres are linked by rigid connectors but exchange volume [42] (Fig. 2 (d)), the details of which will be discussed in Section 3.

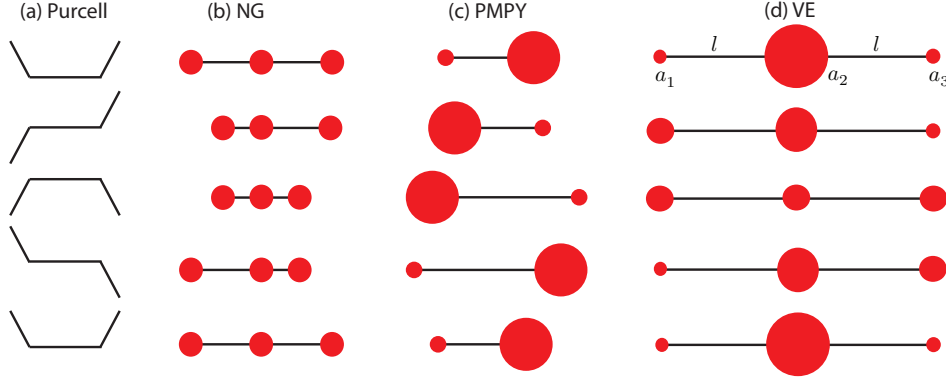


Figure 2: Low Reynolds number swimming models: (a) Purcell's 3-link swimmer [36]; (b) Najafi-Golestanian's 3-sphere model (NG)[31]; (c) Pushmepullyou (PMPY) [7]; (d) The 3-sphere volume-exchange model (VE) [42].

A central problem in the analysis of both biological LRN swimmers and mini-robots is whether a cyclic sequence of deformations results in significant movement, and if such a swimming mode is efficient by some measure. This has been studied for Purcell's swimmer [39], the PMPY swimmer [5] and cilia-based swimming [29, 32]. Lighthill's definition [28] provides one metric of efficiency and several others have been used, but we will introduce a new criterion to measure the performance of LRN swimmers.

Of course in reality the various shape changes that have been analyzed require internal forces that generate the shape changes needed for propulsion of the organism. In biological organisms this *interior* problem involves the biochemical and biophysical changes in the cytoskeleton needed to produce the necessary intracellular forces and shape changes, but here we simply prescribe the shape changes and treat the *exterior* problem. An integrated model that includes sensing the environment and controlling the shape changes so as to move is still beyond reach for even a single-cell organism.

**2. Movement by shape changes – the exterior problem.** The Navier-Stokes equations for an incompressible fluid of density  $\rho$ , viscosity  $\mu$ , and velocity  $\mathbf{u}$  are

$$\rho \frac{\partial \mathbf{u}}{\partial t} + \rho(\mathbf{u} \cdot \nabla) \mathbf{u} = \nabla \cdot \boldsymbol{\sigma} + \mathbf{f}_{\text{ext}} = -\nabla p + \mu \Delta \mathbf{u} + \mathbf{f}_{\text{ext}}, \quad (1)$$

$$\nabla \cdot \mathbf{u} = 0 \quad (2)$$

where  $\boldsymbol{\sigma} = -p\delta + \mu(\nabla \mathbf{u} + (\nabla \mathbf{u})^T)$  is the Cauchy stress tensor and  $\mathbf{f}_{\text{ext}}$  is the external force field. Herein we assume that the swimmer is self-propelled and does not rely on any exterior force, and therefore we require that  $\mathbf{f}_{\text{ext}} = 0$ . The Reynolds number based on a characteristic length scale  $L$  and speed scale  $U$  is  $\text{Re} = \rho LU/\mu$ , and when converted to dimensionless form and the symbols re-defined, the equations read

$$\text{Re}Sl \frac{\partial \mathbf{u}}{\partial t} + \text{Re}(\mathbf{u} \cdot \nabla) \mathbf{u} = -\nabla p + \Delta \mathbf{u}, \quad (3)$$

$$\nabla \cdot \mathbf{u} = 0.$$

Here  $Sl = \omega L/U$  is the Strouhal number and  $\omega$  is a characteristic frequency of the shape changes. When  $Re \ll 1$  the convective momentum term in (3) can be neglected, but the time variation requires that  $ReSl \equiv \omega L^2/\nu \ll 1$ . When both terms are neglected, which we assume throughout, the flow is governed by the Stokes equations

$$\mu \Delta \mathbf{u} - \nabla p = \mathbf{0}, \quad \nabla \cdot \mathbf{u} = 0. \quad (4)$$

We also only consider the propulsion problem in an infinite domain and impose the condition  $\mathbf{u}|_{\mathbf{x} \rightarrow \infty} = \mathbf{0}$  on the velocity.

In the LRN regime time does not appear explicitly, momentum is assumed to equilibrate instantaneously, and bodies move by exploiting the viscous resistance of the fluid. As a result, time-reversible deformations produce no motion, which is the content of the ‘scallop theorem’ [35]. In the absence of external forces due to boundaries or other fields there is no net force or torque on a self-propelled swimmer in the Stokes regime, and therefore movement is a purely geometric process: the net displacement of a swimmer during a stroke is independent of the rate at which the stroke is executed, as long as the Reynolds number remains small enough. Amoebae of the slime mold *Dictyostelium discoideum* have a typical length  $L \sim 25 \mu\text{m}$  and can swim at  $U \sim 3 \mu\text{m}/\text{min}$  [40]. Assuming the medium is water ( $\rho \sim 10^3 \text{kg m}^{-3}$ ,  $\mu \sim 10^{-3} \text{Pa} \cdot \text{s}$ ), and the deformation frequency  $\omega \sim 1/\text{s}$ ,  $Re \sim \mathcal{O}(10^{-6})$  and  $Sl \sim \mathcal{O}(10^{-4})$ . In fact the experiments are done in oil that is significantly more viscous [9], and for similar cells one can neglect both inertial terms.

Suppose that a swimmer occupies the closed compact domain  $\Omega(t) \subset R^n$  ( $n = 2, 3$ ), at time  $t$ , and let  $\partial\Omega(t)$  denote its prescribed time-dependent boundary. A *swimming stroke*  $\Gamma$  is specified by a time-dependent sequence of the boundary  $\partial\Omega(t)$ , and it is *cyclic* if the initial and final shapes are identical, i.e.,  $\partial\Omega(0) = \partial\Omega(T)$  where  $T$  is the period [38]. The swimmers’ boundary velocity  $\mathbf{V}$  relative to fixed coordinates can be written as a part  $\mathbf{v}$  that defines the intrinsic shape deformations, and a rigid motion  $\mathbf{U}$ . If  $\mathbf{u}$  denotes the velocity field in the fluid exterior to  $\Omega$ , then a standard LRN self-propulsion problem is : *given a cyclic shape deformation specified by  $\mathbf{v}$ , solve the Stokes equations subject to*

$$\int_{\partial\Omega(t)} \boldsymbol{\sigma} \cdot \mathbf{n} = \mathbf{0}, \quad \int_{\partial\Omega(t)} \mathbf{r} \wedge (\boldsymbol{\sigma} \cdot \mathbf{n}) = \mathbf{0}, \quad \mathbf{u}|_{\partial\Omega(t)} = \mathbf{V} = \mathbf{v} + \mathbf{U}, \quad \mathbf{u}|_{\mathbf{x} \rightarrow \infty} = \mathbf{0} \quad (5)$$

where  $\mathbf{n}$  is the exterior normal, and the integrals are the force- and torque-free conditions.

In order to treat general shape changes of a cell defined by  $\Omega(t) \in R^3$  with boundary  $\partial\Omega(t)$ , one must solve the exterior Stokes equations (4) for  $\mathbf{u}$ , with a prescribed velocity  $\mathbf{v}(t)$  on  $\partial\Omega(t)$  and subject to the decay conditions  $\mathbf{u} \sim 1/r$  and  $p \sim 1/r^2$  for  $r \rightarrow \infty$ . It is known that the solution has the representation

$$\mathbf{u}(\mathbf{x}) = -\frac{1}{8\pi\mu} \int_{\partial\Omega(t)} \mathbf{G}(\mathbf{x}, \mathbf{y}) \cdot \mathbf{f}(\mathbf{y}) dS(\mathbf{y}) + \frac{1}{8\pi} \int_{\partial\Omega(t)} \mathbf{v}(\mathbf{y}) \cdot \mathbf{T}(\mathbf{y}, \mathbf{x}) \cdot \mathbf{n} dS(\mathbf{y}) \quad (6)$$

where  $\mathbf{G}$  is the free-space Green’s function,  $\mathbf{T}$  is the associated third-rank stress tensor, and  $\mathbf{f} = \boldsymbol{\sigma} \cdot \mathbf{n}$  is the force on the boundary [34]. The constraints that the total force and the total torque vanish determine the center-of-mass translational and angular velocities. When  $\mathbf{x} \in \partial\Omega(t)$  this is an integral equation for the force distribution on the boundary, the solution of which determines the forces needed to produce the prescribed shape changes. The approach is similar in spirit to what has been done for cells crawling on a deformable substrate, where the substrate

deformations are given and the forces exerted by the cell are the solution of a Fredholm integral equation [8, 14].

The free space Green's function or Stokeslet has the form

$$\mathbf{G}(\mathbf{x}, \mathbf{x}_0) = \frac{1}{r} \left[ \mathbf{I} + \frac{\mathbf{r}\mathbf{r}}{r^2} \right] \quad (7)$$

where  $\mathbf{I}$  is the unit second-rank tensor,  $\mathbf{r} = \mathbf{x} - \mathbf{x}_0$ , and  $r = |\mathbf{x} - \mathbf{x}_0|$ . Thus the velocity field generated by a point force  $\mathbf{f}$  at the origin is

$$\mathbf{u}(\mathbf{x}) = \frac{\mathbf{G}(\mathbf{x}, \mathbf{0})}{8\pi\mu} \cdot \mathbf{f} \quad (8)$$

$\mathbf{G}(\mathbf{x}, \mathbf{0})/(8\pi\mu)$  is called the Oseen tensor. Three other basic solutions that are needed are those for a rigid sphere pulled through a quiescent fluid, for a radially expanding or contracting sphere, and for the interaction between two spheres.

When a sphere of radius  $a$  is pulled through a quiescent fluid with a steady force  $\mathbf{F}$  under no-slip conditions at the surface, the resulting flow field is given by

$$\mathbf{u}(\mathbf{r}) = \mathbf{F} \cdot \left(1 + \frac{a^2}{6} \nabla^2\right) \frac{\mathbf{G}(\mathbf{x}, \mathbf{x}_s)}{8\pi\mu} = \frac{\mathbf{F}}{8\pi\mu r} \cdot \left[ \mathbf{I} + \frac{\mathbf{r}\mathbf{r}}{r^2} + \frac{a^2}{3r^2} \left[ \mathbf{I} - 3\frac{\mathbf{r}\mathbf{r}}{r^2} \right] \right] \quad (9)$$

where  $\mathbf{x}_s$  is position of the center of the sphere and  $\mathbf{r} = \mathbf{x} - \mathbf{x}_s$ . The second term represents the degenerate quadrupole needed to satisfy the no-slip boundary condition at  $r = a$ , but it is small when  $a/r \ll 1$ . The resulting velocity of the sphere is given by Stoke's law [24]

$$\mathbf{F} = 6\pi\mu a \mathbf{U}. \quad (10)$$

This can be obtained directly from (6) by setting  $\mathbf{v} = 0$  in the second integral, expanding the Green's function, and defining the total force on the sphere as

$$\mathbf{F} = \int_{\partial\Omega} \mathbf{f}(\mathbf{y}) dS(\mathbf{y}). \quad (11)$$

A second basic solution is the velocity field  $\mathbf{u}$  produced by a radially expanding sphere, which can be generated by a point source at the center  $\mathbf{x}_s$  of the sphere [34]. The corresponding velocity is

$$\mathbf{u} = \alpha \frac{\mathbf{r}}{r^3} \quad (12)$$

where  $\mathbf{r} = \mathbf{x} - \mathbf{x}_s$  and  $\alpha$  is a constant to be determined. The no-slip boundary condition at the surface  $r = a$  requires that

$$\mathbf{u}(\mathbf{r}) \Big|_{|\mathbf{r}|=a} = \frac{da}{dt} \frac{\mathbf{r}}{a} \quad (13)$$

and therefore  $\alpha = \dot{a}a^2$ , and

$$\mathbf{u} = \dot{a} \left( \frac{a}{r} \right)^2 \frac{\mathbf{r}}{r} = \frac{\dot{v}}{4\pi r^2} \hat{\mathbf{r}}, \quad (14)$$

where  $v = 4\pi a^3/3$  is the volume of the sphere and  $\hat{\mathbf{r}} = \mathbf{r}/r$ . By combining equations (9, 13) we obtain the velocity field for the combination of the pulled and expanding sphere, namely [7]

$$\mathbf{u}(\mathbf{r}; a, \mathbf{F}, \dot{v}) = \frac{1}{24\pi\mu r} \left[ \left(3 + \frac{a^2}{r^2}\right) \mathbf{F} + 3\left(1 - \frac{a^2}{r^2}\right) (\mathbf{F} \cdot \hat{\mathbf{r}}) \hat{\mathbf{r}} \right] + \frac{\dot{v}}{4\pi r^2} \hat{\mathbf{r}}. \quad (15)$$

The last basic solution needed involves the interaction between two spheres<sup>1</sup>. Suppose that the  $i$ th ( $i = 1, 2$ ) sphere has radius  $a_i(t)$ , is centered at  $\mathbf{x}_i(t)$  and is subjected to a drag force  $\mathbf{F}_i(t)$  due to its motion. The translational velocity of the  $i$ th sphere consists of two parts:  $\mathbf{U}_{i,0} = (6\pi\mu a_i)^{-1}\mathbf{F}_i$  that results from the drag force  $\mathbf{F}_i$  exerted on  $i$ , and the other a perturbation part  $\delta\mathbf{U}_i$  that is due to the flow generated by the other sphere. In particular, since the other sphere is translating and expanding,  $\delta\mathbf{U}_i$  can be further decomposed into two parts:  $\delta\mathbf{U}_i^t$  due to the translation of the other sphere, and  $\delta\mathbf{U}_i^e$  that results from its radial expansion. Hence we have the following decomposition of the translational velocity of the  $i$ th sphere.

$$\mathbf{U}_i = \frac{\mathbf{F}_i}{6\pi\mu a_i} + \delta\mathbf{U}_i^t + \delta\mathbf{U}_i^e \quad (16)$$

Here  $\delta\mathbf{U}_i^t$  arises from a flow given by equation (9) and is given by

$$\begin{aligned} \delta\mathbf{U}_i^t &= \left(1 + \frac{a_i^2}{6}\nabla^2\right)\mathbf{u}(\mathbf{r})\Big|_{\mathbf{r}=\mathbf{x}_i-\mathbf{x}_j} \\ &= \frac{1}{8\pi\mu l} \left[ \left(1 + \frac{a_i^2 + a_j^2}{3l^2}\right)\mathbf{I} + \left(1 - \frac{a_i^2 + a_j^2}{l^2}\right)\frac{\mathbf{l}\mathbf{l}}{l^2} \right] \mathbf{F}_j \end{aligned} \quad (17)$$

where  $\mathbf{l} = \mathbf{x}_i - \mathbf{x}_j$  and  $l = |\mathbf{x}_i - \mathbf{x}_j|$  [10]. The velocity  $\delta\mathbf{U}_i^e$  is resulted from a flow given by equation (13):

$$\delta\mathbf{U}_i^e = \left(1 + \frac{a_i^2}{6}\nabla^2\right)\mathbf{u}(\mathbf{r})\Big|_{\mathbf{r}=\mathbf{x}_i-\mathbf{x}_j} = \mathbf{u}(\mathbf{x}_i - \mathbf{x}_j) = \frac{a_j^2 \dot{a}_j}{l^3} \mathbf{l} \quad (18)$$

Altogether,  $\delta\mathbf{U}_i^t$  and  $\delta\mathbf{U}_i^e$  induce a higher-order perturbation in  $\mathbf{U}$ , but as we shall see, these terms are neglected in the existing analyses of linked-spheres.

Next we use these solutions in the analysis of various models, and we begin with the pure volume-exchange (VE) model.

**3. The 3-sphere volume-exchange model.** Some cells produce membrane protrusions called blebs that emerge when the membrane detaches from the cortex locally and the excess internal pressure forces fluid into the bleb [17, 33]. When this occurs repeatedly over a cell surface, as in Fig. 3(a), it may result in an oscillatory motion of the cell. In Fig. 3(a) the cell blebs profusely with little net translation, whereas Fig. 3(b) shows a motile, blebbing *Dictyostelium discoideum* cell. If bleb formation is restricted to the leading edge as in (b), forward motion is driven by contraction of the cortical network at the rear of the cell. In either case one can understand the dynamics in terms of mass or volume exchange between different parts of the cell. The protrusions are usually approximately hemispherical and thus a linked-sphere model may be a good choice for a study of blebbing. However most existing linked-spheres models require significant changes in the length of the connecting links, which is not realistic in blebbing cells. This led us to develop a model that better describes blebbing dynamics [42].

In a minimal VE model there are three spheres linked by two rigid, mass-less arms of fixed length  $l$  (Fig. 2(d)). A sphere can only expand or contract in the radial direction (i.e.,  $a_i = a_i(t)$ ), and can only exchange mass with its neighbor(s), i.e., 1 with 2 and 2 with 3 but not 1 with 3. There is little evidence that swimming cells exchange significant material with the surrounding fluid, and thus we impose mass

<sup>1</sup>For simplicity we assume that the interactions in a general configuration of spheres are pairwise additive.

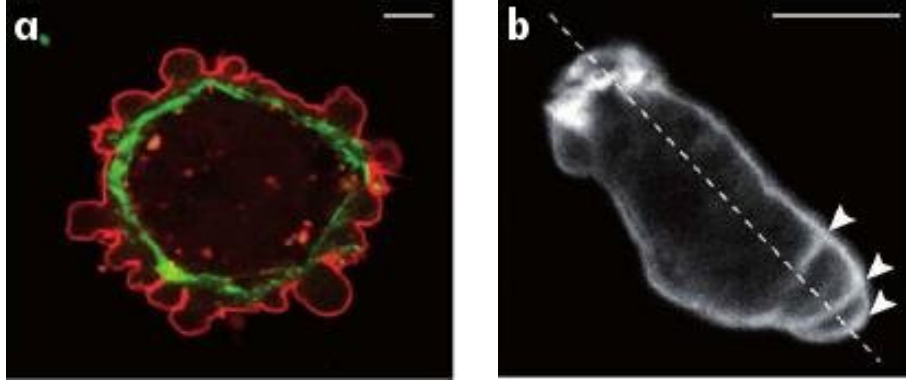


Figure 3: (a) Blebbing on a melanoma cell: myosin (green) localizes under the blebbing membrane (red) (from[15]) (b) The actin cortex of a blebbing Dd cell migrating to the lower right. Arrowheads indicate the successive blebs and arcs of the actin cortex (from[43]).

conservation on the ensemble. We are primarily concerned with the fluid-structure interaction and for simplicity we assume that the density in all three spheres is the same constant, in which case the mass conservation is equivalent to volume conservation. We also ignore dissipation within cells, and with these constraints, it is easily seen from the “scallop theorem” [35] that a cyclic two-sphere model cannot swim, since it has only one degree of freedom. Therefore a minimal model must comprise at least three spheres.

The velocity field is given by equation (15), and to obtain asymptotic solutions, we assume that the distance  $l$  between either pair of neighboring spheres is larger than the radii  $a_i$  ( $i = 1, 2, 3$ ), i.e.,  $a_i/l \ll 1$ , which simplifies the computation yet captures basic aspects of the movement of blebbing cells. The VE model is linear, thus the velocity  $\mathbf{U}_i$  of the  $i$ th sphere and the force  $\mathbf{F}_i$  exerted on the  $i$ th sphere are all along the  $x$ -direction.

$$\mathbf{U}_i = U_i \mathbf{e}_x, \quad \mathbf{F}_i = F_i \mathbf{e}_x$$

Because the Stokes problem is linear, the velocity  $U_i$  of each sphere is given by equations (16, 17, 18), wherein we only retain the leading order terms in the perturbations  $\delta \mathbf{U}_i^t$  and  $\delta \mathbf{U}_i^e$ . The asymptotic solution for the  $U_i$  is given by

$$U_1 \sim \frac{F_1}{6\pi\mu a_1} + \left( \frac{F_2}{4\pi\mu l} - \frac{\dot{v}_2}{4\pi l^2} \right) + \left( \frac{F_3}{8\pi\mu l} - \frac{\dot{v}_2}{16\pi l^2} \right) \quad (19)$$

$$U_2 \sim \frac{F_2}{6\pi\mu a_2} + \left( \frac{F_1}{4\pi\mu l} + \frac{\dot{v}_1}{4\pi l^2} \right) + \left( \frac{F_3}{4\pi\mu l} - \frac{\dot{v}_3}{4\pi l^2} \right) \quad (20)$$

$$U_3 \sim \frac{F_3}{6\pi\mu a_3} + \left( \frac{F_1}{8\pi\mu l} + \frac{\dot{v}_1}{16\pi l^2} \right) + \left( \frac{F_2}{4\pi\mu l} + \frac{\dot{v}_2}{4\pi l^2} \right) \quad (21)$$

where  $v_i = 4\pi a_i^3/3$  and  $\dot{v}_2 = -\dot{v}_1 - \dot{v}_3$ . Since the connecting arms have fixed length  $l$ ,  $U_1 = U_2 = U_3$ , which defines the translational velocity  $U$  of the swimmer. Since the swimmer is linear it is necessarily torque-free, and the force-free constraint is

$$F_1 + F_2 + F_3 = 0. \quad (22)$$

The volume conservation constraint reads

$$\dot{v}_1 + \dot{v}_2 + \dot{v}_3 = 0 \quad (23)$$

and (19 – 23) lead to the following asymptotic solution for the swimming velocity of the model [42].

$$U = \frac{(a_1 + a_2 - \frac{3}{4}a_3)\dot{v}_1 - (a_3 + a_2 - \frac{3}{4}a_1)\dot{v}_3}{4\pi l^2(a_1 + a_2 + a_3)} \quad (24)$$

Next, we consider the power  $P \equiv \int_0^T f(t)U(t)dt$  required to propel the swimmer. The stress on the surface of the expanding sphere is  $\sigma = \mu\dot{v}/(\pi a^3)$  [7], and therefore the power required to expand one sphere is

$$4\pi a^2 \sigma \dot{a} = \sigma \dot{v} = \frac{4\mu}{3v} \dot{v}^2 \quad (25)$$

Therefore the total instantaneous power expended by the swimmer in transferring volumes between the spheres is

$$P = \frac{4\mu}{3} \left[ \frac{\dot{v}_1^2}{v_1} + \frac{\dot{v}_2^2}{v_2} + \frac{\dot{v}_3^2}{v_3} \right] = \frac{\mu}{\pi} \left[ \left( \frac{1}{a_1^3} + \frac{1}{a_2^3} \right) \dot{v}_1^2 + \frac{2}{a_3^3} \dot{v}_1 \dot{v}_3 + \left( \frac{1}{a_2^3} + \frac{1}{a_3^3} \right) \dot{v}_3^2 \right]. \quad (26)$$

Finally we define the performance of a stroke  $\Gamma$  as the ratio of the translation per cycle to the energy expended in a cycle.

$$e = \frac{|\int_0^T U(t)dt|}{\int_0^T P(t)dt} \quad (27)$$

This has units of 1/force.

When the volume changes are small several conclusions can be reached analytically [42, 41]. Since a swimming stroke is a closed path in the  $v_1 - v_3$  plane or equivalently, a closed path in the  $a_1 - a_3$  plane, we find the following relation between the differential displacement  $\bar{d}x$  and the differential controls  $(da_1, da_3)$  from (24).

$$\bar{d}X = \frac{\pi}{l^2} \left[ a_1^2 \left( 1 - \frac{7}{4} \frac{a_3}{a_1 + a_2 + a_3} \right) da_1 - a_3^2 \left( 1 - \frac{7}{4} \frac{a_1}{a_1 + a_2 + a_3} \right) da_3 \right] \quad (28)$$

Here  $\bar{d}X > 0$  represents an infinitesimal displacement to the right in Fig. 2(d). The bar in  $\bar{d}X$  indicates that the differential displacement is not an exact differential.

To determine the direction of swimming, note that from equation (28) we may assume, without loss of generality, that  $da_3 = 0$  and  $da_1 > 0$ , which means that sphere 3 does not change, and sphere 1 is expanding while sphere 2 is contracting. For  $a_2$  large enough so that  $1 - 7a_3/(a_1 + a_2 + a_3) > 0$  always holds, we have  $\bar{d}X > 0$ , which means that the swimming direction is from sphere 1 to sphere 2. Hence we have the following conclusion, which also applies to the PMPY swimmer.

**Conclusion 1.** *When only one pair of adjacent spheres is involved in volume exchange, and when the central sphere is large enough, the direction of swimming is always from the expanding sphere to the contracting one.*

Next, using Stokes' theorem, the translation  $\delta X$  corresponding to an infinitesimal closed loop is

$$\delta X = \frac{7\pi}{4l^2} \left[ a_1^2 \partial_{a_3} \frac{a_3}{a_1 + a_2 + a_3} + a_3^2 \partial_{a_1} \frac{a_1}{a_1 + a_2 + a_3} \right] da_1 \wedge da_3 \quad (29)$$



where  $da_1 \wedge da_3$  denotes the signed area enclosed by the loop. From this one can show the following.

**Conclusion 2.** *For strokes such that  $\Gamma$  is homotopic to the unit circle, increasing the stroke amplitude will increase the net translation of the stroke, while increasing the initial radius  $a_{20}$  of the central sphere (with  $a_{10}$  and  $a_{30}$  unchanged) will decrease the net translation. Moreover, we have the approximation*

$$|X(\Gamma)| \sim \frac{\varepsilon}{l} \text{Area}(\Omega)$$

where  $\varepsilon \sim a_i/l$  and  $\Omega$  is the region enclosed by  $\Gamma$  and  $\text{Area}(\Omega)$  is its signed area.

The proof of this is given in [41].

**3.1. Numerical computations.** Next we prescribe cycles of shape changes in the controls  $(\dot{a}_1, \dot{a}_3)$  and compute the displacement and performance measure numerically. In particular, we investigate how the following characteristics of the system affect the net translation  $X = \int_0^T U(t)dt$  and the performance  $e$  of the swimmer after a full cycle ( $T = 1$ ).

1.  $L$ , which measures the distance between a pair of neighboring sphere;
2.  $r_1, r_2$ , which measure the amplitude of shape deformations;
3.  $s$ , which measures the size of the central sphere.

We use the following protocol in varying these parameters.

$$\text{Arm length (fixed)} : \quad l_1 = l_2 = L$$

$$\text{Controls} : \quad a_1(t) = R_0 + r_1 \cos 2\pi t, \quad a_3(t) = R_0 + r_3 \sin 2\pi t,$$

$$\text{Radius of the central sphere} : \quad a_2(0) = s, \quad a_2(t) = \left( \frac{3}{4\pi} V_{\text{tot}} - a_1(t)^3 - a_3(t)^3 \right)^{\frac{1}{3}}$$

We consider three cases.

- I** First, we set  $r_1 = r_3 = 1$ ,  $R_0 = 2$  and  $s = 3$ , and test different values of  $L$ , i.e., arm length (Fig. 4(a,b)). Fig. 4(c) gives the initial profile of the swimmers with  $L = 10$  and  $L = 50$ , respectively. Fig. 4(a,b) show that both the translation  $X$  and the performance  $e$  decrease as the arm length increases. That is to say, with a fixed amount of body mass, a too long body is not a good strategy for swimming. The effect on the translation  $X$  can be seen from equation (24) and Conclusion 2, with a fixed stroke rendering the same  $\text{Area}(\Omega)$ , the translation  $X$  scales in the order of  $\varepsilon l^{-1} = al^{-2}$ . Hence as the arm length  $L$  increases,  $X$  decreases quickly. As for performance  $e$  (equation (27)), it is the ratio of translation to energy over a cycle, with power  $P$  given by equation (26), from which we clearly see that the arm length  $L$  does not enter into the expression of  $P$ . Hence  $e$  decays similarly to  $X$ , namely, in the order of  $l^{-2}$ .
- II** Next, we set  $L = 50, s = 10, R_0 = 10$ , and test different values of  $r_1$  and  $r_3$  (Fig. 4(c,d)), i.e., the stroke amplitude. Fig. 4(e) gives the initial profile of the swimmers with  $r_3 = 1$  always, but  $r_1 = 1$  or  $r_1 = 9$ , respectively. From Fig. 4(c) we see that The translation increases as either  $r_i$  increases, but if one of  $r_i$  is small, the increase of translation due to the other  $r_j$  is small. This can be explained by Conclusion 2, in general a large  $r_1$  or/and  $r_3$  indicate a large stroke, i.e., a large  $\text{Area}(\Omega)$ , which clearly induces a large translation  $X$  — except that when one of  $r_i$  is small, then no matter how large the other  $r_i$  is, we have  $\text{Area}(\Omega) \sim 0$ , which results in a  $X \sim 0$ . As for performance, it is difficult to obtain a general analysis between  $e$  and  $\text{Area}(\Omega)$ , yet Fig. 4(c) indicates that  $e$  has the similar behavior as  $X$  (though maybe not to the same order), i.e.,  $e$  increases as either  $r_i$  increases, if the other  $r_i$  is not too small.

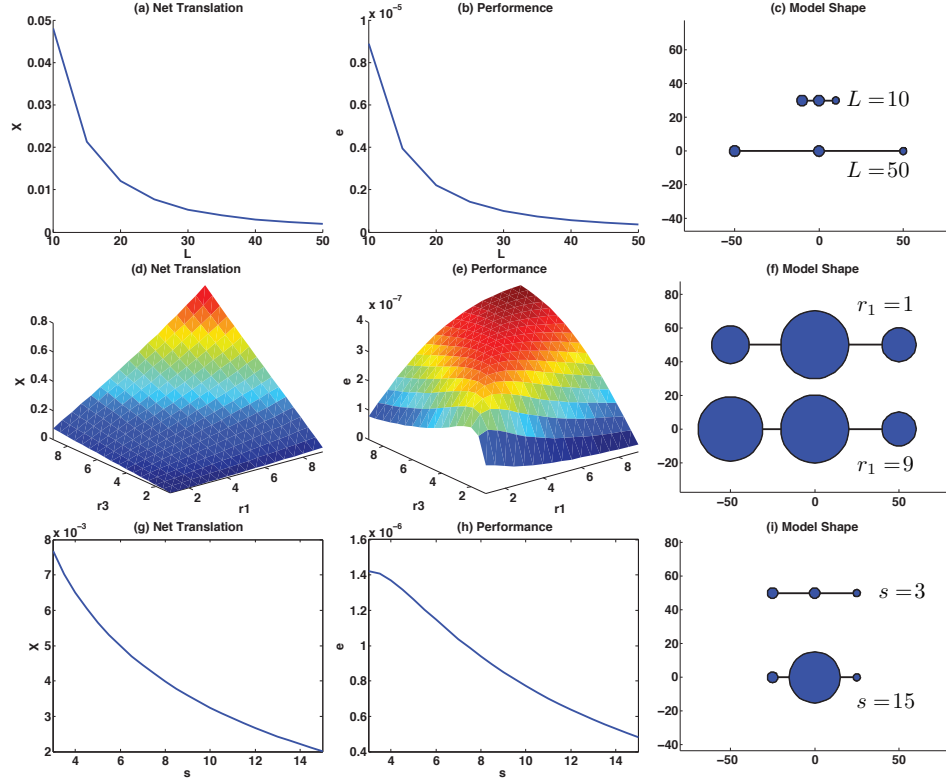


Figure 4: (a,b) Translation  $X$  and performance  $e$  as a function of the fixed arm length  $L$ . (c) The initial shape of the swimmer when  $L = 10$  or  $L = 50$  in simulations shown in a& b. (d,e) Translation  $X$  and performance  $e$  as a function of the stroke amplitude  $(r_1, r_3)$ . (f) The initial shape of the swimmer when  $r_1 = 1$  or  $r_1 = 9$  in simulations shown in (d,e). Notice that although both  $r_1$  and  $r_3$  determine the stroke amplitude, the initial shape is only related to  $r_1$ . (g,h) Translation  $X$  and performance  $e$  in relation of the (initial) size of the central sphere  $s$ . (i) The initial shape of the swimmer when  $s = 3$  or  $s = 15$  in simulations shown in (g,h). The scales are the same for panels (c,f,i).

**III** Finally we set  $L = 25, r_1 = r_3 = 1$  and  $R_0 = 2$ , and test different values of  $s$  (Fig. 4(e,f)), i.e., the (relative) size of the central sphere to the side spheres. Here we would like to point out such a test can be considered a complement to the test of stroke amplitude. Consider that we may scale the total volume of the whole object to be the same with respect to different values of  $s$ , then a model with a small central sphere (Fig. 4(i),  $s = 3$ ) is translated to one with a large stroke, and on the other hand a large central sphere (Fig. 4(i),  $s = 15$ ) corresponds to a swimmer with a small stroke. Hence the results can be predicted from previous discussion and are shown in Fig. 4(e,f): both the translation and the performance decrease as the initial radius of the central sphere is increased. Yet we illustrate such behavior in regard to  $s$ . Observe equation (29) and we find that with both the stroke amplitude  $da_1 \wedge da_3$  and the arm length  $L$  fixed,  $X$  is proportional to the following quantity:

$$a_1^2 \partial_{a_3} \frac{a_3}{a_1 + a_2 + a_3} + a_3^2 \partial_{a_1} \frac{a_1}{a_1 + a_2 + a_3} \quad (30)$$

which clearly decreases as the central sphere gets bigger. On the other hand, equation (26) indicates that a bigger central sphere results in small power  $P$ . To evaluate

the effect of the size of the central sphere on the performance  $e$ , we conduct an asymptotic analysis with the scenario  $a_1, a_3 \ll a_2$ . In such a case, the quantity given by equation (30) approximates 0, then equation (29) shows that  $\delta X \sim 0$ . However from equation (26) we obtain the following behavior  $P$  when  $a_1, a_3 \ll a_2$ :

$$P \sim \frac{\mu}{\pi} \left[ \frac{1}{a_1^3} \dot{v}_1^2 + \frac{1}{a_3^3} \dot{v}_3^2 \right]$$

which in general does not vanish. Hence as the ratio of average translation to average power, the performance  $e$  vanishes in the scenario  $a_1, a_3 \ll a_2$ .

In conclusion, in order to reach longer net translation  $X$  or better performance  $e$ , the 3-sphere volume-exchange model should be designed so that *the connecting arm is short, more mass are exchanged among the spheres though the cycle, and the central sphere should not be big comparing to the two side spheres*.

**4. A comparison of the three linked-sphere swimmers.** Here we compare the performance of the three linked-sphere swimmers: the NG 3-sphere model, the pushmepullyou (PMPY) and the VE model. A summary of the analysis that leads to the velocity and power of the NG and PMPY models can be found in Appendix A and in [31, 19, 7]. To standardize the comparison between them, we stipulate that the total volume in all spheres are the same for each model, and the stroke amplitudes are the same. We prescribe strokes for each model as follows.

- **NG:**

$$R_1 = R_2 = R_3 = 2r_G$$

$$l_1(t) = L + \cos(2\pi t), \quad l_2(t) = L + \sin(2\pi t)$$

- **Pushmepullyou:**

$$R_1 = 2r_P + \cos(2\pi t)$$

$$R_2(0) = 2r_P, \quad R_1^3 + R_2^3 = \frac{3}{4\pi} V_{\text{tot}}$$

$$l(t) = L + \sin(2\pi t)$$

- **Volume-exchange (VE):**

$$l_1 = l_2 = L$$

$$R_1(t) = 2r_V + \cos(2\pi t), \quad R_3(t) = 2r_V + \sin(2\pi t)$$

$$R_2(0) = 2r_V, \quad R_1^3 + R_2^3 + R_3^3 = \frac{3}{4\pi} V_{\text{tot}}$$

where scales  $r_G, r_P, r_V$  are chosen so that the total volume of all spheres in each swimmer are the same. Without loss of generality, we may choose  $r_G = 1$ .

First, the velocity  $U(t)$  and the power  $P(t)$  within a cycle that result from the above prescribed strokes are given in Figs 5(a–d), for  $L = 6$  or 30, respectively. For translation, comparing Fig. 5(a) and (c) we see that  $U(t)$  for PMPY does not change much, while it almost vanishes for NG and VE when  $L = 30$ . On the other hand,  $P(t)$  in Fig. 5(b) and Fig. 5(d) are quite much similar.

Moreover, we find that the PMPY model is clearly superior to the others (Fig. 5(e,f)), in regard to both translation and performance over the entire range of  $L$ , even when  $L \rightarrow \infty$ . The reason can be found in the asymptotic solutions of  $U$  and  $P$  for the three swimmers. While the leading term of  $U$  for PMPY is  $\mathcal{O}(1)$ , it is  $\mathcal{O}(l^{-1})$  and  $\mathcal{O}(l^{-2})$  for NG and VE, respectively. The leading order term in the power  $P$  is  $\mathcal{O}(1)$  (equation (26)) for all three swimmers, hence the arm length  $L$  does not have much influence on the power or the performance  $e$ . The leading order term of  $e$  is

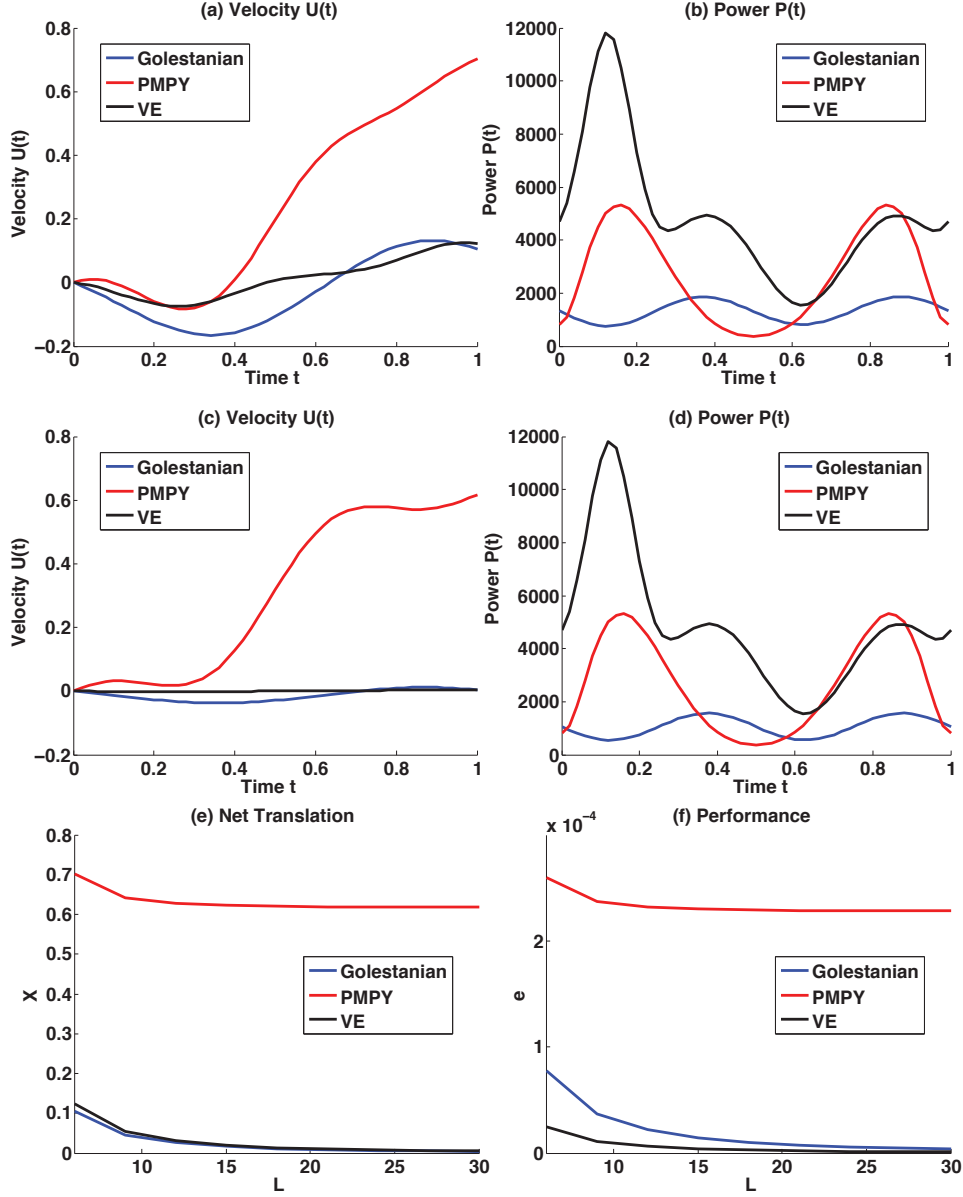


Figure 5: A comparison of the three linked-sphere swimmers. (a,b)  $U(t)$  and  $P(t)$  of the swimmers within a cycle with  $L = 6$ . (c,d)  $U(t)$  and  $P(t)$  of the swimmers within a cycle with  $L = 30$ . (e,f) Net translation  $X$  and performance  $e$  of the three swimmers with different values of  $L$ .

the same as that of  $U$ , i.e.,  $\mathcal{O}(1), \mathcal{O}(l^{-1}), \mathcal{O}(l^{-2})$  for PMPY, Golestanian and VE, respectively.

##### 5. Mixed controls result in more net translation and better performance.

All three models have two degrees of freedom, which are of two types – a change in the arm length  $\dot{l}$ , or a change in the sphere radius  $\dot{a}$ . Different combinations of the

controls result in different swimming behaviors, and from the results above we find that the best choice is the mixed strategy, *i.e.*,  $(\dot{l}, \dot{R})$ , which is adopted by PMPY. A combination of the same kind —  $(\dot{l}_1, \dot{l}_2)$  or  $(\dot{R}_1, \dot{R}_2)$  — is not advantageous, and they produce comparable net translation and performance (Fig. 5).

The priority of the mixed strategy is based on the following two principles:

1.  $\dot{l}$  results in a velocity with leading order  $\mathcal{O}(1)$ , while the leading order that results from  $\dot{R}$  is only  $\mathcal{O}(l^{-2})$ . Hence to increase the net translation, one should incorporate a change in arm length.
2. The leading order terms in the velocity  $U(t)$  should not be, or even approximate, an exact differential, because they then make no or little contribution to the net translation.

We have discussed the first principle above, which clearly explains why PMPY is better than the other two swimmers. However this does not explain why the net translation behaves similar for NG and VE, with leading order terms that scale like  $\mathcal{O}(l^{-1})$  and  $\mathcal{O}(l^{-2})$ , respectively. In fact, it is only in the case that all three spheres are of equal size that the velocity scales like  $\mathcal{O}(l^{-1})$  for the NG swimmer. When tspheres are of different sizes are involved,  $U(t)$  will actually scale as  $\mathcal{O}(1)$ , *i.e.*, the same as  $U(t)$  in the PMPY model. However, the net translation  $X$  still turns out to be of order  $\mathcal{O}(l^{-2})$ , which is the same as for the VE swimmer.

To understand this, we analyze the asymptotic solution of  $U(t)$  for an NG swimmer which is approximated to the order  $\mathcal{O}(l^{-1})$  (equation (A1), [19]). The equation is complex, but it can be written in the following form.

$$U = A_0 \dot{l}_1 + B_0 \dot{l}_2 + \left( \frac{A_1^{(1)}}{l_1} + \frac{A_1^{(2)}}{l_2} + \frac{A_1^{(12)}}{l_1 + l_2} \right) \dot{l}_1 + \left( \frac{B_1^{(1)}}{l_1} + \frac{B_1^{(2)}}{l_2} + \frac{B_1^{(12)}}{l_1 + l_2} \right) \dot{l}_2 + \mathcal{O}\left(\frac{1}{l^2}\right) \quad (31)$$

where all coefficients  $A_i^{(\alpha)}, B_i^{(\alpha)}$  are functions of  $a_1, a_2, a_3$  only and do not depend on  $l_1, l_2$  or time  $t$ .

The leading order term of  $U$ , denoted as  $U_{(0)}$ , is the combination

$$U_{(0)} = A_0 \dot{l}_1 + B_0 \dot{l}_2$$

and the integral over a whole cycle gives

$$X_{(0)} = \int_0^T U_{(0)} dt = \int_0^T (A_0 \dot{l}_1 + B_0 \dot{l}_2) dt = A_0 l_1 \Big|_{t=0}^{t=T} + B_0 l_2 \Big|_{t=0}^{t=T} = 0. \quad (32)$$

Next, the  $\mathcal{O}(l^{-1})$  term of  $U$ , which we denote  $U_{(1)}$ , is given by the following.

$$U_{(1)} = \left( \frac{A_1^{(1)}}{l_1} + \frac{A_1^{(2)}}{l_2} + \frac{A_1^{(12)}}{l_1 + l_2} \right) \dot{l}_1 + \left( \frac{B_1^{(1)}}{l_1} + \frac{B_1^{(2)}}{l_2} + \frac{B_1^{(12)}}{l_1 + l_2} \right) \dot{l}_2$$

In general, the integral  $\int_0^T U_1 dt$  does not vanish, but we have the relation

$$l_i(t) = L + \delta l_i(t)$$

where  $L$  is the fixed part and  $\delta l_i$  is the deformation part. When  $L$  is sufficiently large, so as to ensure that the higher-order interactions between spheres are negligible, we have that  $\delta l_i \ll L$ , and thus  $U_{(1)}$  can be approximated as

$$U_{(1)} \sim \left( \frac{A_1^{(1)}}{L} + \frac{A_1^{(2)}}{L} + \frac{A_1^{(12)}}{2L} \right) \dot{l}_1 + \left( \frac{B_1^{(1)}}{L} + \frac{B_1^{(2)}}{L} + \frac{B_1^{(12)}}{2L} \right) \dot{l}_2$$

Thus again,

$$\begin{aligned}
X_{(1)} &\sim \int_0^T U_{(1)} dt \\
&= \left( \frac{A_1^{(1)}}{L} + \frac{A_1^{(2)}}{L} + \frac{A_1^{(12)}}{2L} \right) \int_0^T \dot{i}_1 dt + \left( \frac{B_1^{(1)}}{L} + \frac{B_1^{(2)}}{L} + \frac{B_1^{(12)}}{2L} \right) \int_0^T \dot{i}_2 dt \\
&= 0
\end{aligned} \tag{33}$$

From equations (32, 33), we see that although in general the  $\mathcal{O}(1)$  and  $\mathcal{O}(l^{-1})$  terms do not vanish in  $U(t)$ , the  $\mathcal{O}(1)$  term is an exact differential and the  $\mathcal{O}(l^{-1})$  term is approximately an exact differential, and hence the net translation  $X \sim \mathcal{O}(l^{-2})$ . This is the same as the leading order that results from varying the radii in the VE model.

Fig. 6(a,b) give  $U(t)$  within one cycle for four NG swimmers, whose radii are given in Fig. 6(c), with  $L = 10$  or  $L = 100$ . Again, to make a fair comparison we require the total volume of all three spheres in each swimmer are the same. We do not use equation (A1) in [19] to solve for  $U(t)$ , instead we numerically solve the whole system (equations (34 - 36)). From Fig. 6(a,b) we see that for the same swimmer, the amplitude of  $U(t)$  within a cycle is almost of the same scale when  $L = 10$  or  $100$ , yet the net translation is very small with either value of  $L$ . However we do observe that among different choices of the sphere sizes, net translation favors the equal sized spheres (S0) – *i.e.*, S0 results in the most net translation yet it requires the least amplitude of  $U(t)$  among the four swimmers.

On the other hand, for PMPY the leading term in  $U(t)$  is

$$U_{(0)} = \frac{a_1 - a_2}{2(a_1 + a_2)} \dot{i} \sim \mathcal{O}(1)$$

which is not an exact differential, and as a result, the leading order term in the net translation gives

$$X_{(0)} = \int_0^T \frac{a_1 - a_2}{2(a_1 + a_2)} \dot{i} dt \sim \mathcal{O}(1)$$

in general, which explains the better performance of the PMPY swimmer as compared with the Golestanian or VE swimmer.

**6. Discussion.** We have compared the three most widely-studied discrete swimmers and have shown that the PMPY swimmer performs best under the imposed conditions. This conclusion is important for the design of mini-robots, but of course real systems are more complex, and as we indicated earlier, the VE model is a more realistic model of cellular motion. An analysis of continuum models of swimmers that more accurately reflect actual shape changes will be reported elsewhere.

**Appendix A. A summary of the NG and PMPY models.** The NG swimmer (Fig. 2(b)) consists of three spheres with radii  $a_i$  ( $i = 1, 2, 3$ ) and two connecting arms with length  $l_i(t)$  ( $i = 1, 2$ ) [30, 18, 1]. While the spheres are rigid, the connecting arms can stretch or contract. In the case when  $a_i/l \ll 1$ , the velocities of the spheres ( $U_i$ ) are related to the forces exerted on the spheres ( $F_i$ ) via the Oseen

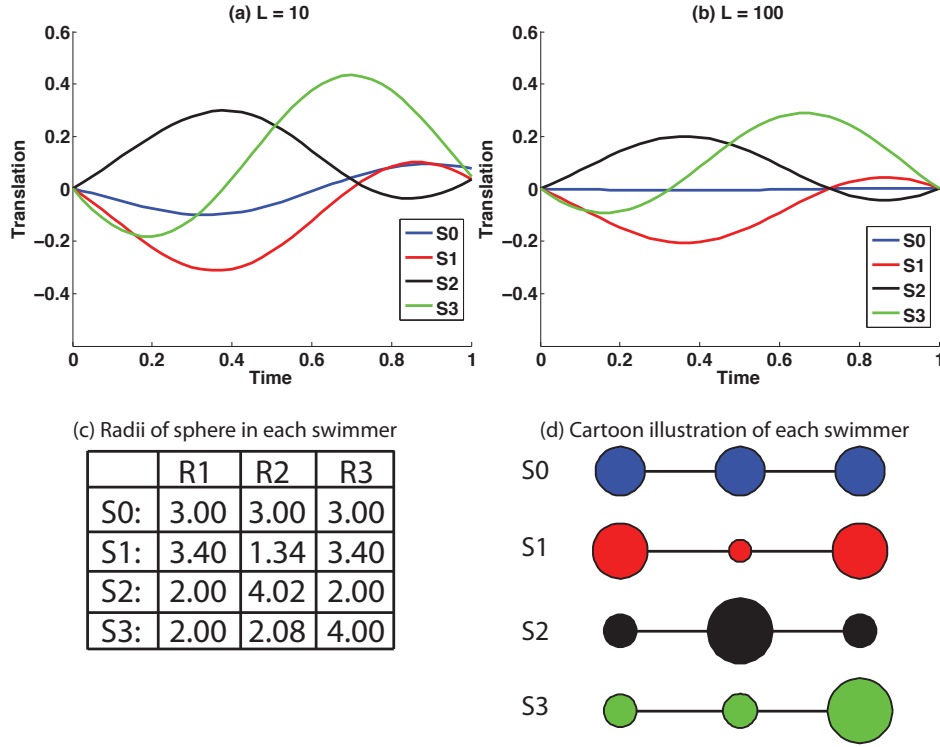


Figure 6: (a)  $U(t)$  of four Golestian swimmers, with  $L = 10$ . (b)  $U(t)$  of four Golestian swimmers, whose spheres have correspondingly the same size as in (a), but with  $L = 10$ . (c) The radius of each sphere in each swimmer of (a,b). (d) Initial shapes of the four swimmer (with  $L = 15$  for better visualization effects).

tensor:

$$U_1 = \frac{F_1}{6\pi\mu a_1} + \frac{F_2}{4\pi\mu l_1} + \frac{F_3}{4\pi\mu(l_1 + l_2)} \quad (34)$$

$$U_2 = \frac{F_1}{4\pi\mu l_1} + \frac{F_2}{6\pi\mu a_2} + \frac{F_3}{4\pi\mu l_2} \quad (35)$$

$$U_3 = \frac{F_1}{4\pi\mu(l_1 + l_2)} + \frac{F_2}{4\pi\mu l_2} + \frac{F_3}{6\pi\mu a_3} \quad (36)$$

The velocities are related via the following relations:

$$U_2 - U_1 = \dot{l}_1, \quad U_3 - U_2 = \dot{l}_2 \quad (37)$$

The system is force-free

$$F_1 + F_2 + F_3 = 0 \quad (38)$$

and equations (34 - 38) are a closed system. The velocity of the whole swimmer is defined as

$$U = \frac{1}{3}(U_1 + U_2 + U_3) \quad (39)$$

In the case that the spheres are of equal size, we have the asymptotic solution

$$U = \frac{a}{6} \left[ \frac{\dot{l}_2 - \dot{l}_1}{l_1 + l_2} + 2 \left( \frac{\dot{l}_1}{l_2} - \frac{\dot{l}_2}{l_1} \right) \right]. \quad (40)$$

The power consumption of the swimmer comes from dragging the spheres, thus

$$P = F_1 U_1 + F_2 U_2 + F_3 U_3 \quad (41)$$

and in the case that the spheres are of equal size the above equation simplifies to

$$\frac{P}{4\pi\mu a} = \left[ 1 + \frac{a}{l_1} - \frac{a}{2l_2} + \frac{a}{l_1 + l_2} \right] \dot{l}_1^2 + \left[ 1 - \frac{a}{2l_1} + \frac{a}{l_2} + \frac{a}{l_1 + l_2} \right] \dot{l}_2^2 \quad (42)$$

$$+ \left[ 1 - \frac{a}{2l_1} - \frac{a}{2l_2} + \frac{5a}{2(l_1 + l_2)} \right] \dot{l}_1 \dot{l}_2. \quad (43)$$

The PMPY swimmer (Fig. 2(c)) consists of two spheres with radii  $a_i(t)$  ( $i = 1, 2$ ) and one connecting arms with length  $l(t)$ . The spheres can expand or contract in the radial direction, and the connecting arms can stretch or contract. When  $a_i/l \ll 1$ , the velocities of the spheres ( $U_i$ ) are related to the forces exerted on the spheres ( $F_i$ ) via the Oseen tensor

$$U_1 = \frac{F_1}{6\pi\mu a_1} + \frac{a_1^2}{l^2} \dot{a}_1 \quad (44)$$

$$U_2 = \frac{F_2}{6\pi\mu a_2} + \frac{a_2^2}{l^2} \dot{a}_2. \quad (45)$$

The velocities are related via the following relation.

$$U_2 - U_1 = \dot{l} \quad (46)$$

Again, the system is force-free

$$F_1 + F_2 = 0 \quad (47)$$

and the total volume of the two spheres is conserved

$$a_1^2 \dot{a}_1 + a_2^2 \dot{a}_2 = 0. \quad (48)$$

Equations (44 - 48) are a closed system and the velocity of the swimmer is

$$U = \frac{1}{2}(U_1 + U_2) = \frac{a_1 - a_2}{2(a_1 + a_2)} \dot{l} + \frac{a_1^2}{l^2} \dot{a}_1. \quad (49)$$

The power consumption  $P(t)$  of the swimmer comprises two parts:  $P_{\text{drag}}$  that results from the drag force on the spheres, which is given by

$$P_{\text{drag}} = F_1 U_1 + F_2 U_2 \quad (50)$$

and  $P_{\text{exp}}$  that results from the radial expansion of the swimmers

$$P_{\text{exp}} = 16\pi\mu(a_1 \dot{a}_1^2 + a_2 \dot{a}_2^2). \quad (51)$$

Hence the power expended is given by

$$P = 6\pi\mu \left( \frac{1}{a_1} + \frac{1}{a_2} \right)^{-1} \dot{l}^2 + 16\pi\mu(a_1 \dot{a}_1^2 + a_2 \dot{a}_2^2). \quad (52)$$

## References



- [1] Alexander, GP, Pooley, CM, and Yeomans, JM. 2009. Hydrodynamics of linked sphere model swimmers. *Journal of Physics: Condensed Matter*, **21**, 204108.
- [2] Alouges, François and DeSimone, Antonio and Lefebvre, Aline, 2008. Optimal strokes for low Reynolds number swimmers: an example. *Journal of Nonlinear Science*, **18**(3), 277–302
- [3] Alouges, François and DeSimone, Antonio and Lefebvre, Aline, 2009. Optimal strokes for axisymmetric microswimmers. *The European Physical Journal E: Soft Matter and Biological Physics*, **28**(3), 279–284
- [4] Alouges, François and DeSimone, Antonio and Heltai, Luca, 2011. Numerical strategies for stroke optimization of axisymmetric microswimmers. *Mathematical Models and Methods in Applied Sciences*, **21**(02), 361–387
- [5] Avron, J. E., Gat, O., and Kenneth, O. 2004. Optimal swimming at low Reynolds numbers. *Phys. Rev. Lett.*, **93**(18), 186001.
- [6] Avron, JE and Raz, O. 2008. A geometric theory of swimming: Purcell’s swimmer and its symmetrized cousin. *New Journal of Physics*, **10**, 063016.
- [7] Avron, JE, Kenneth, O., and Oaknin, DH. 2005. Pushmepullyou: An efficient micro-swimmer. *New Journal of Physics*, **7**, 234.
- [8] Barentin, C., Sawada, Y., and Rieu, J. P. 2006. An iterative method to calculate forces exerted by single cells and multicellular assemblies from the detection of deformations of flexible substrates. *Eur Biophys J*, **35**(4), 328–339.
- [9] Barry, N. P. and Bretscher, M. S. 2010. Dictyostelium amoebae and neutrophils can swim. *PNAS*, **107**(25), 11376.
- [10] Batchelor, G. K. 1976. Brownian diffusion of particles with hydrodynamic interaction. *J. Fluid Mech.*, **74**(part 1), 1–29.
- [11] Batchelor, GK. 1970. Slender-body theory for particles of arbitrary cross-section in Stokes flow. *Journal of Fluid Mechanics*, **44**(03), 419–440.
- [12] Becker, LE, Koehler, SA, and Stone, HA. 2003. On self-propulsion of micro-machines at low Reynolds number: Purcell’s three-link swimmer. *Journal of fluid mechanics*, **490**(1), 15–35.
- [13] Binamé, F., Pawlak, G., Roux, P., and Hibner, U. 2010. What makes cells move: requirements and obstacles for spontaneous cell motility. *Molecular BioSystems*, **6**(4), 648–661.
- [14] Butler, J. P., Tolic-Norrelykke, I. M., Fabry, B., and Fredberg, J. J. 2001. Traction fields, moments, and strain energy that cells exert on their surroundings. *Am J Physiol Cell Physiol*, **282**, C595–C605.
- [15] Charras, G. T. and Paluch, E. 2008. Blebs lead the way: how to migrate without lamellipodia. *Nat Rev Mol Cell Biol*, **9**, 730–736.
- [16] Cox, RG. 1970. The motion of long slender bodies in a viscous fluid Part 1. General theory. *Journal of Fluid mechanics*, **44**(04), 791–810.
- [17] Fackler, O.T. and Grosse, R. 2008. Cell motility through plasma membrane blebbing. *The Journal of cell biology*, **181**(6), 879–884.
- [18] Golestanian, R. and Ajdari, A. 2007a. Analytic results for the three-sphere swimmer at low Reynolds number. *Arxiv preprint arXiv:0711.3700*.
- [19] Golestanian, R. and Ajdari, A. 2007b. Analytic results for the three-sphere swimmer at low Reynolds number. *Arxiv preprint arXiv:0711.3700*.
- [20] Hancock, GJ. 1953. The self-propulsion of microscopic organisms through liquids. *Proceedings of the Royal Society of London. Series A. Mathematical and Physical Sciences*, **217**(1128), 96–121.

- [21] Johnson, R.E. 1980. An improved slender-body theory for Stokes flow. *Journal of Fluid Mechanics*, **99**(2), 411–431.
- [22] Johnson, RE and Brokaw, C.J. 1979. Flagellar hydrodynamics. A comparison between resistive-force theory and slender-body theory. *Biophysical journal*, **25**(1), 113–127.
- [23] Keller, J.B. and Rubinow, S.I. 1976. Slender-body theory for slow viscous flow. *J. Fluid Mech*, **75**(4), 705–714.
- [24] Kim, S. and Karrila, S. J. 1991. *Microhydrodynamics: Principles and Selected Applications*. Vol. 507. Butterworth-Heinemann Boston.
- [25] Lämmermann, T., Bader, B. L., Monkley, S. J., Worbs, T., Wedlich-Söldner, R., Hirsch, K., Keller, M., Förster, R., Critchley, D. R., Fässler, R., et al.. 2008. Rapid leukocyte migration by integrin-independent flowing and squeezing. *Nature*, **453**, 51–55.
- [26] Lauga, E. and Powers, T. R. 2009. The hydrodynamics of swimming microorganisms. *Repts. on Prog. in Phys.*, **72**, 096601.
- [27] Lighthill, J. 1976. Flagellar hydrodynamics: the John von Neumann lecture, 1975. *SIAM review*, pages 161–230.
- [28] Lighthill, M.J. 1952. On the squirming motion of nearly spherical deformable bodies through liquids at very small Reynolds numbers. *Communications on Pure and Applied Mathematics*, **5**(2), 109–118.
- [29] Michelin, Sébastien and Lauga, Eric. 2010. Efficiency optimization and symmetry-breaking in a model of ciliary locomotion. *Physics of Fluids (1994-present)*, **22**(11), 111901.
- [30] Najafi, A. and Golestanian, R. 2004a. A simplest swimmer at low Reynolds number: Three linked spheres. *Arxiv preprint cond-mat/0402070*.
- [31] Najafi, A. and Golestanian, R. 2004b. A simplest swimmer at low Reynolds number: Three linked spheres. *Arxiv preprint cond-mat/0402070*.
- [32] Osterman, Natan and Vilfan, Andrej. 2011. Finding the ciliary beating pattern with optimal efficiency. *Proceedings of the National Academy of Sciences*, **108**(38), 15727–15732.
- [33] Paluch, E., Piel, M., Prost, J., Bornens, M., and Sykes, C. 2005. Cortical actomyosin breakage triggers shape oscillations in cells and cell fragments. *Biophysical journal*, **89**(1), 724–733.
- [34] Pozrikidis, C. 1992. *Boundary Integral and Singularity Methods for Linearized Viscous Flow*. Cambridge Univ Pr. ISBN 0-521-40693-5.
- [35] Purcell, E. 1977a. Life at low Reynolds number. *Amer.J.Physics*, **45**, 3–11.
- [36] Purcell, E.M. 1977b. Life at low Reynolds number. *Am. J. Phys*, **45**(1), 3–11.
- [37] Renkawitz, J. and Sixt, M. 2010. Mechanisms of force generation and force transmission during interstitial leukocyte migration. *EMBO reports*, **11**(10), 744–750.
- [38] Shapere, Alfred and Wilczek, Frank. 1989. Geometry of self-propulsion at low Reynolds number. *J. Fluid Mech.*, **198**, 557–585.
- [39] Tam, Daniel and Hosoi, Annete E. 2007. Optimal stroke patterns for Purcells three-link swimmer. *Physical Review Letters*, **98**(6), 068105.
- [40] Van Haastert, P. J. M. 2011. Amoeboid Cells Use Protrusions for Walking, Gliding and Swimming. *PloS one*, **6**(11), e27532.
- [41] Wang, Q. 2012. *Modeling of Amoeboid Swimming at Low Reynolds Number*. Ph.D. thesis, University of Minnesota.

- [42] Wang, Q., Hu, J., and Othmer, H. G. 2012. *Natural Locomotion in Fluids and on Surfaces: Swimming, Flying, and Sliding*. Frontiers in Applications of Mathematics. New York: Springer Verlag. Pages 197–206. Chap. Models of low Reynolds number swimmers inspired by cell blebbing, pages 197–206.
- [43] Yoshida, K. and Soldati, T. 2006. Dissection of amoeboid movement into two mechanically distinct modes. *J. Cell Sci.*, **119**, 3833–3844.

Received

Accepted

*E-mail address:* [qixuanw@uci.edu](mailto:qixuanw@uci.edu) and [othmer@math.umn.edu](mailto:othmer@math.umn.edu)